International Symposium
On Turbulence and Shear Flow
Phenomena (TSFP-9)
June 30 - July 3, 2015 *Melbourne, Australia*

TURBULENT DRAG REDUCTION DUE TO THE WAVY SURFACES OF A TRUNCATED PYRAMID

Mitsuhiro Shintani
Technology Development Dept.
Yamamoto Kogaku Co.,LTD.
Higashi-Osaka City, Osaka 577-0056, Japan
shintani@yamamoto-kogaku.co.jp

Keisuke Maeda
Dept. of Mechanical and System Engineering
Kyoto Institute of Technology
Sakyo-ku, Kyoto 606-8585, Japan
m3623049@edu.kit.ac.jp

Yoshimichi Hagiwara
Dept. of Mechanical and System Engineering
Kyoto Institute of Technology
Sakyo-ku, Kyoto 606-8585, Japan
yoshi@kit.ac.jp

ABSTRACT

The total drag and the wall shear stress were measured for truncated pyramids covered with flat surfaces or wavy surfaces in an open channel at a high Reynolds number. The total drag acting on the samples was measured from the strain of the thin metal strips supporting the samples. The value of the total drag for the sample covered with the wavy surfaces was 7.9% lower than that of the sample covered with flat surfaces. The wall shear stress acting on the surface of each sample was estimated from the mean velocity profile. There was a reduction in friction drag of 8.8×10^{-4}(N) for the truncated pyramids covered with wavy surfaces when compared with the pyramid with flat surfaces. There was a 1.8% reduction in friction drag when comparing the difference in the total drag between the flat surfaces and the wavy surfaces.

INTRODUCTION

We have problems of depletion of fossil fuels and global warming in recent years. Many studies on energy-saving have been actively conducted in various fields in order to solve these problems. It is possible to reduce consumption of resources and suppress greenhouse gases produced by the combustion of fossil fuels through the application of energy-saving technologies. The reduction of drag acting on a body from fluid flow is a typical example of these technologies.

Our research group has focused on the folds of skin which appear on a dolphin's chest and abdominal areas only when the dolphin swims at a high speed. Former members of our group carried out the total drag measurement of a wavy plate which mimicked the skin of a dolphin (Yoshitake et al., 2008). They found that the total drag of a wavy plate increased and the friction drag of this plate decreased when compared with a flat plate. In addition, they found that a circulating flow appeared intermittently at the valley of the wavy surface if the value of the ratio a/λ of amplitude to wavelength was $a/\lambda=0.035$.

Other members of our group carried out the total drag measurement for an angle-wavy plate (Ozaki et al., 2009). In addition other members of our group researched the relationship between the difference of the amplitude of a wavy surface to a flat plate and the total drag (Kuroda et al., 2009). However, in these studies the wavy surfaces were on a flat plate. Therefore, studies in the case where the basal plane is the surface of a three-dimensional object have not yet been conducted.

Two of the present authors previously measured the total drag of swimming goggles whose surfaces were shaped in wavy forms (Shintani et al., 2012). The tops of the wavy forms were set at the same position on the flat surface, and the surfaces of the wavy forms were caved from a flat surface with an amplitude of a=0.1mm. The results showed a reduction of total drag when compared with that in the case of goggles without a wavy form, although the samples of both types of goggles had the same projected area to the main flow direction. However, nobody has elucidated the mechanism for a wavy form which affects a total drag.

Building on the results of these previous studies, the purpose of this study is to establish a method that more efficiently reduces drag for a three dimensional object whose surfaces are shaped in some kind of wavy form. In this study, we carry out the measurement of truncated pyramids since these are a relatively simple three dimensional object. We measure the total drag and the change of the flow in the vicinity of the wavy surfaces on the pyramids.

EXPERIMENTAL SETUP

Apparatus

Figure 1 shows the apparatus. Water flows from the upper tank to the chamber through a pipe and a valve for adjusting the flow rate. After the water in the chamber passes a part which straightens the flow and a part which narrows the flow, it flows into the open channel whose size is 2000 mm in length, 270 mm in width and 150 mm

in height. The water in the open channel then flows into the lower tank and is returned to the upper tank with a submersible pump. A tripping wire and an emery paper were placed at the channel inlet in order to advance the development of a turbulent boundary layer flow. The bottom wall of the open channel from the inlet to the downstream end of the test section except for the area where the test sample was positioned was covered with a natural rubber sheet in order to reduce the drag and the turbulence of the flow which were generated by a thickness of a stainless steel plate which was placed a test sample. The test section was placed at 1150 mm. The x-, y- and z-axes were arranged respectively in the streamwise direction, upward direction and spanwise direction.

The Reynolds number, based on the mean velocity u_e outside the turbulent boundary layer and the streamwise distance from the inlet of the channel, was 1.2×10^6.

The Kolmogorov length scale l_K and Kolmogorov time scale t_K were estimated by using the friction velocity and the dissipation rate of turbulent kinetic energy. The dissipation rate near a flat wall was calculated from the DNS result obtained by Iwamoto et al. (2002). l_K and t_K were 0.027 mm and 0.67 ms respectively.

Test samples

Figure 2 (a) shows a truncated pyramid with flat surfaces. Figure 2 (b) shows a truncated pyramid whose surfaces were shaped in a wavy form. The wavy form of the surface is shown in Figure 3. The wavy forms were shaped by changing the value of the amplitude a and the wavelength λ. The value of a, λ and the ratio a/λ for each wavy surface is described in Table 1. The top of the wavy form was located on the edge of each face of the pyramid. Therefore, all of these test samples have the same projected area to the mainstream direction of the flow.

The test samples were fixed with double-sided tape on a T-shaped stainless-steel plate whose length in the streamwise direction was 300 mm. These test samples were placed in the position of 150 mm from the forefront edge of the stainless-steel plate. We hollowed out parts of the samples, and these are indicated with dotted lines in Figure 2, and fitted a stainless-steel block into these parts in order to increase the gross weight of test samples. The weight of each of the test samples is shown in Table 1.

Table 1 a , λ , a/λ and weight of each sample

	a (mm)	λ (mm)	a/λ	Weight (g)
model 1	---	---	---	44.0
model 2	0.10	2.86	0.035	43.1
model 3	0.06	1.72	0.035	43.4
model 4	0.30	8.58	0.035	41.2
model 5	0.10	1.72	0.058	43.0
model 6	0.10	8.58	0.012	43.0

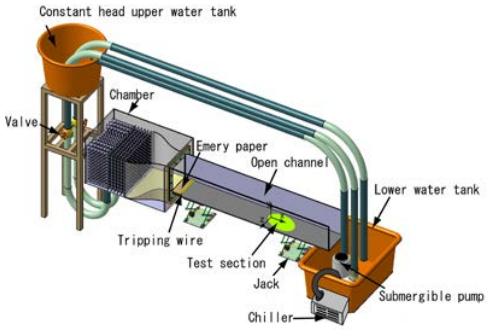

Fig.1 Apparatus

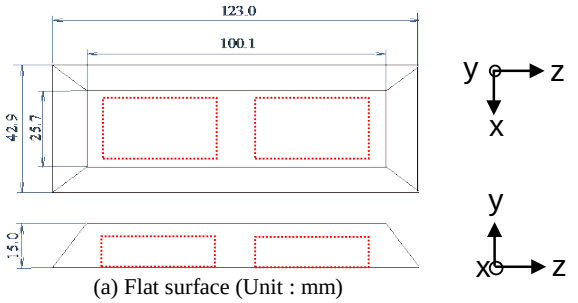

(a) Flat surface (Unit : mm)

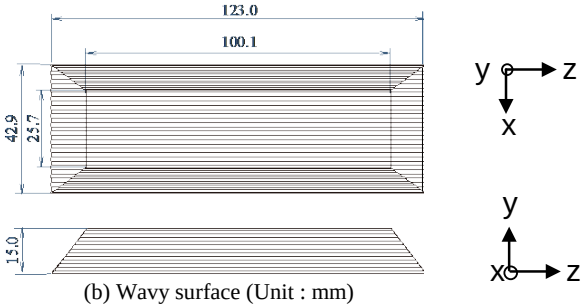

(b) Wavy surface (Unit : mm)

Fig.2 Test samples

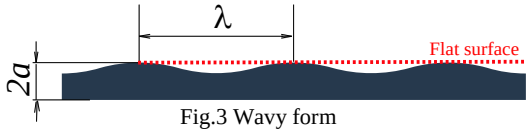

Fig.3 Wavy form

MEASUREMENT PROCEDURES

Total drag

The measurement system for the total drag acting on the test sample is indicated in Figure 4. The stainless-steel plates with the test samples were not fixed to the bottom wall so that they could slide freely to the streamwise direction. The stainless-steel plate was supported by two vertical cantilevers, which were made of phosphor-bronze strips. One end of each cantilever was clamped above the free surface. The other end of each cantilever made contact with one of the edges of a U-shaped part. This part was fixed to the edge of each wing of the stainless-steel plate. The edge of the stainless-steel plate at the downstream side was fixed by a stop.

When we removed the stop slowly, the test sample received drag from the flow and moved slightly to the downstream direction. Then, the cantilevers were deflected slightly by the movement of the test sample. We measured the strain at a location on each cantilever by

using a strain gauge. The gauges were attached to the cantilevers and connected to bridge circuits. The outputs from the circuits were recorded on a PC. We carried out a calibration experiment to obtain the relationship between the outputs from the circuits and the load. We also calculated the total drag acting on the test sample with the calibration lines.

Many particles of 0.25 mm in diameter were arranged between the lower surface of the stainless-steel plate and the bottom surface of the channel in order to reduce the friction force between the stainless-steel plate and the bottom of the channel. In order to reduce errors caused by impinging flow to the cantilevers, the cantilevers were positioned inside the indented parts of the sidewall. These indented parts were covered with a plastic sheet. We set the water depth to 54 mm and the water temperature at 17±2 degrees Celsius.

Velocity field

We used tracer particles for the visualization of the turbulent flow. The upper limit of frequency f_x, which these particles can respond to fluid sinusoidal fluctuations, was estimated to be 460 Hz and 1200 Hz when the value of the ratio of the density of a particle ρ_P to the density of water ρ_W was ρ_P/ρ_W=1.10 and 1.05 respectively if the diameter of a particle was 0.050 mm. This was estimated using the equations obtained by Hjelmfelt Jr. and Mockris (1966). The density and the range of particle diameter was 1.03 g/cm^3 and 0.048-0.052 mm respectively. The ratio ρ_P/ρ_W was ρ_P/ρ_W=1.03 in this study. In addition, the frequency estimated from the Kolmogorov time scale was $1/t_K$=1482Hz. The frequency which these particles can respond to fluid sinusoidal fluctuations quadratically increased as the density ratio of a particle to water approached 1. We estimated the upper limit of frequency as f_x=1540. Therefore, these particles can respond to fluid sinusoidal fluctuations. Thus, the tracer particles adopted in the present study are reasonable.

The velocity measurement system is shown in Figure 5. The light from an Nd:YVO_4 laser was used as the light source. The laser beam was expanded with a plano-convex cylindrical lens and a plano-concave lens in order to obtain a laser light sheet. The laser light sheet passed though a slit of 5 mm in width and provided illumination from above the open channel. Scattered light from the particles was captured with a CMOS camera (Photron, FASTCAM 1024-PCI). The captured images were directly recorded in a PC. Table 2 shows the image-capturing conditions.

We adopted the following three-step processes in order to calculate velocity vectors with a PTV (Particle Tracking Velocimetry) method from the images including the scattered light (Kitagawa et al., 2007).

(1) The particle-mask correlation method, developed by Etoh et al., (1999), was used to remove any weak scattered light from particles in the images.

(2) The PTV (Particle Tracking Velocimetry) technique based on the velocity gradient tensor method, proposed by Ishikawa et al., (2000), was applied to the preprocessed images for obtaining velocity vectors. In this method, the matrix including the velocity gradient tensor was calculated for pairs of neighboring particles in a specific region around a single particle.

(3) The sum of the square of errors in the matrix was evaluated.

This procedure was repeated for all the candidate particles until the sum reached its minimum value. This method has the advantage of accurately reproducing strongly-deformed velocity fields.

The velocities of the particles were redistributed to the grid points of 14 × 50. The velocity of a particle was simply shifted to the nearest grid point in the redistribution procedure. The uncertainty of the velocity was 0.04 m/s for u_e=1.13m/s. This shows that the measured velocity was accurate.

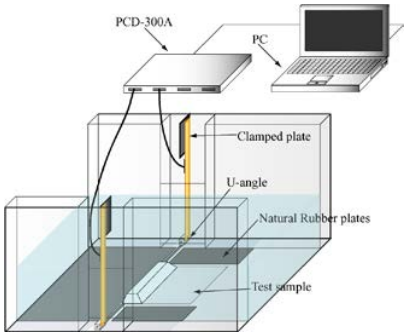

Fig.4 Measurement system of total drag

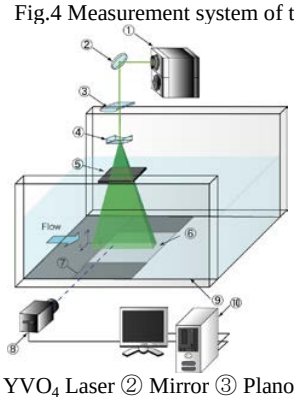

① YVO_4 Laser ② Mirror ③ Plano-convex lens
④ Plano-concave lens ⑤ Slit ⑥ Test plate
⑦ Natural rubber ⑧ C-MOS camera
⑨ Acrylic open channel ⑩ PC
Fig.5 Velocity measurement system

Table 2 Image-capturing conditions

---	PTV	Path line
Pixel numbers	1024×336	1024×1024
Frame rate [fps]	3000	60
Shutter speed [s]	1/9000	1/125
Laser power [A]	25.0	8.0
Resolution [mm/pixel]	(uphill face) 0.051 (top face) 0.028 (downhill face) 0.056	---

RESULTS AND DISCUSSION

Total drag

Figure 6 shows the total drag for each sample. The error bar shows the maximum and minimum value of results for three measurements.

The value of the total drag for the truncated pyramid covered with flat surfaces (model1) was highest. The value of the total drag for model2 was lowest. It was 7.9% lower than that of model1. The value of the total drag for model4 was highest among the samples covered with wavy surfaces.

Figure 7 shows the time changes in the total drag. Table 3 shows the time-averaged values and the RMS values of total drag. The difference of total drag for all samples when compared with the case of model1 was higher than the RMS value. Therefore, we found that this difference was not the result of an error in measurement but was an effect caused by wavy surfaces.

Firstly, we compare model4 and model6 whose surfaces were shaped in a wavy form of λ=8.58 mm. The total drag for model4 was higher than that of model6 whose wavelength was the same as the wavelength of model4. Therefore, we found that the increase in the total drag for model4 was caused by the amplitude being changed into a large value.

Secondly, we compare model2, model3 and model4 whose surfaces were shaped in a wavy form of a/λ=0.035. The total drag for model4 was higher than that for model2. In addition, although model3 had a small amplitude, the total drag for this model was not the lowest among all the samples.Therefore, we found that the total drag was effectively reduced when the amplitude was a certain level, and that this effect was reduced if the amplitude was increased too much.

Thirdly, we compare model2, model5 and model6 whose surfaces were shaped in a wavy form of a=0.10 mm. The total drag for model2 was the lowest among these three models. The total drag for model5 whose wavelength was shorter than model2, and model6 whose wavelength was longer than that of model2, were higher than the total drag for model2. Therefore, we found that the value of the total drag was effectively reduced when the value of the ratio was a/λ=0.035.

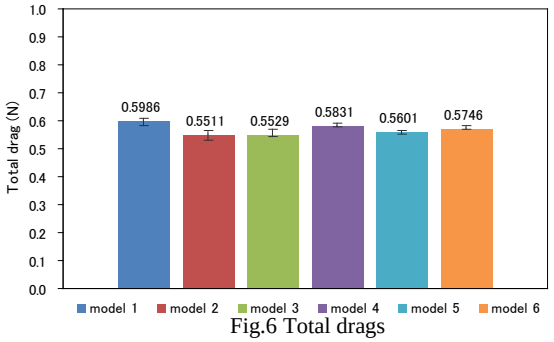

Fig.6 Total drags

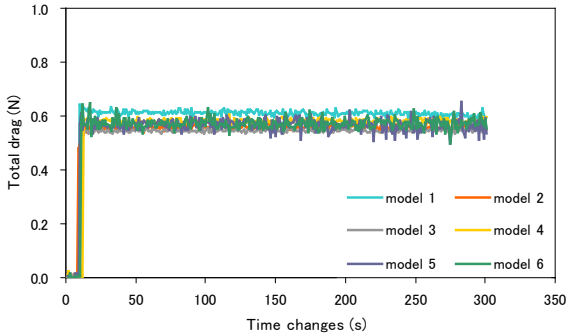

Fig.7 Time changes in total stain profiles

Table 3 Total drags and RMS

Test Sample	Total drag (N)	RMS (N)
model 1	0.599	0.007
model 2	0.551	0.006
model 3	0.553	0.005
model 4	0.583	0.006
model 5	0.560	0.027
model 6	0.575	0.020

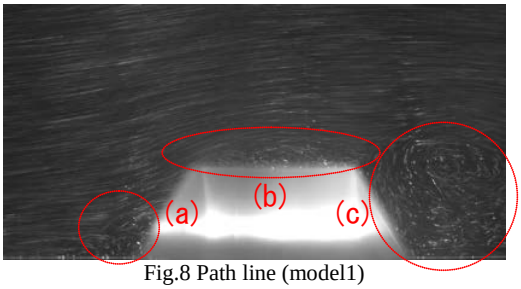

Fig.8 Path line (model1)

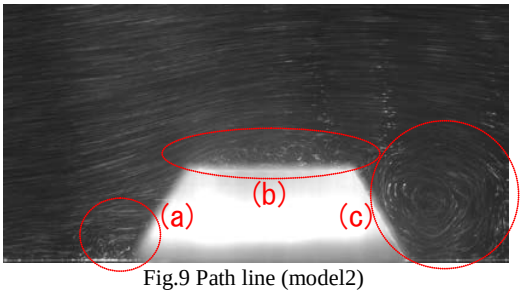

Fig.9 Path line (model2)

Pathline

The flow around the truncated pyramid was visualized with pathline method for model1 and model2. Table 2 shows the image-capturing conditions. Figures 8 and 9 show snapshots of visualized flow. There was no significant difference between the flow in the case of the flat surface and that in the case of the wavy surface at (a) the uphill face, (b) the top face and (c) the downhill face. Also, a vortex appeared intermittently. This was small at the uphill face (a) and large at the downhill face (c) for both the samples. There was a strong flow to the streamwise direction above the top face of the truncated pyramid. The vortex appeared at irregular intervals between the top face and the strong flow.

Velocity field

We carried out a calculation of velocity vectors of the flow near the wall of the uphill face, the top face and the downhill face for model1 and model2. Figure 10 shows the regions for which velocity vectors were calculated.

We measured velocity vectors at the regions (1), (2) and (3) for the uphill face and at the regions (4), (5) and (6) for the top face and at the regions (7), (8) and (9) for the downhill face.

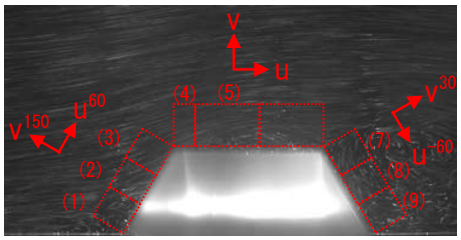

Fig.10 Measurement area

Figure 11 shows the mean velocity of u^{60} and v^{150}. The mean velocity of u^{60} at region (1) near the wall was negative for both model1 and model2. These results show that a vortex appeared at region (1), which is consistent with the results shown in Figs. 8 and 9. The mean velocity of u^{60} for model1 at region (1) became positive at y^{uphill}=1.4 mm above the wall. On the other hand, the mean velocity of u^{60} for model2 became positive at y^{uphill}=2.3 mm. The mean velocity of model2 near the wall was higher than that of model1. Therefore, the flow for model2 at region (1) occurred to a direction in which the total drag was reduced.

The increase in the velocity at region (2) near the wall for model1 was higher than that of model2. The mean velocity of model2 at this position was also lower than that of model1. Therefore, we deduced that the mean velocity of the uphill face was reduced due to the wavy form. The mean velocity at region (3) was similar to that at region (2).

The mean velocity of v^{150} for model1 at region (1) was negative. This negative velocity was increased by a strong flow to the streamwise direction at a position far from the wall. On the other hand, the mean velocity of v^{150} for model2 was negative at y^{uphill}=1.4 mm from the wall. We deduced that the wavy surfaces contributed to a reduction of the total drag.

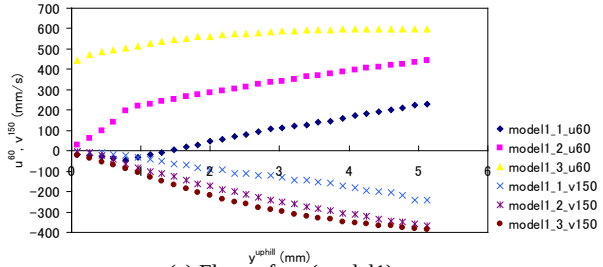

(a) Flat surface (model1)

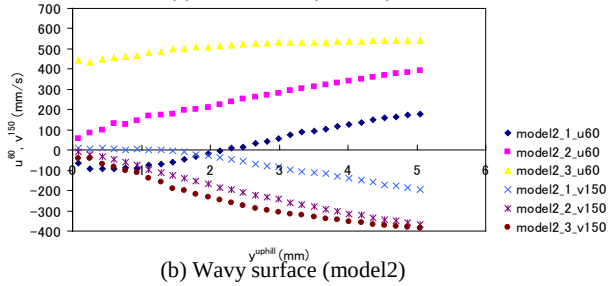

(b) Wavy surface (model2)

Fig.11 Mean velocity profiles (uphill face)

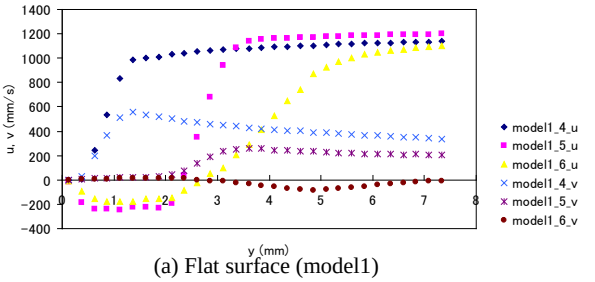

(a) Flat surface (model1)

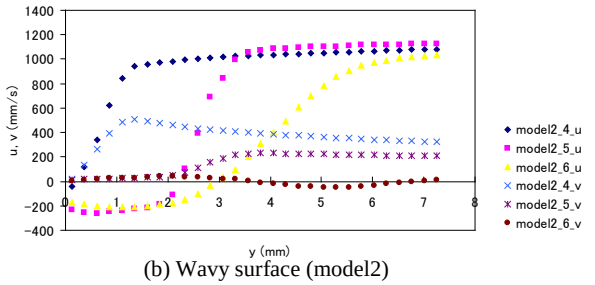

(b) Wavy surface (model2)

Fig.12 Mean velocity profiles (top face)

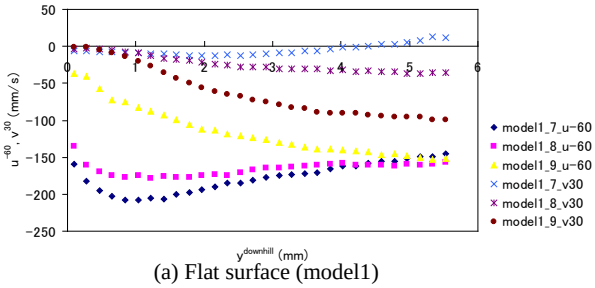

(a) Flat surface (model1)

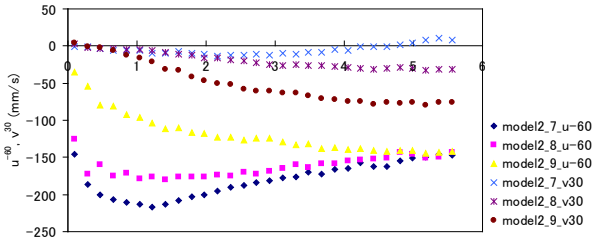

(b) Wavy surface (model2)

Fig.13 Mean velocity profiles (downhill face)

Figure 12 shows the mean velocities of u and v. The mean velocities of u near the wall at the top face for both model1 and model2 were negative in regions (5) and (6). The mean velocities of v near the wall at the top face for both samples were positive in a region of $2<y<4$ mm above the wall at region (5). These mean velocities were negative in a region of $4<y<6$ mm above the wall in region (6). These results showed that a vortex appeared between the top face and a strong flow above the wall. This is the same as that discussed for Figs. 8 and 9.

Figure 13 shows the mean velocities of u^{-60} and v^{30} near the downhill face. The mean velocities of u^{-60} and v^{30} near the wall for both model1 and model2 were negative in all the regions. This result showed that a vortex

appeared at the rear of the downhill face, which was consistent with the results shown in Figs. 8 and 9.

Wall Shear Stress

We compared the wall shear stresses of the uphill face, the top face and the downhill face for model1 with those of model2. The wall shear stresses of the side faces were not able to be measured, so that we were not able to consider the wall shear stresses of the side walls. The wall shear stress was calculated from the velocity at an adjacent point to the wall and the equation $\tau_W = \mu \cdot du/dy$.

Tables 4 and 5 show the wall shear stresses and nomal stresses for each surface.

Table 4 Wall shear stress

surface	region	model1	model2
		τ_W (Pa)	τ_W (Pa)
uphill face	region (1)	-0.099	-0.437
	region (2)	0.278	0.407
	region (3)	2.373	2.261
top face	region (4)	0.021	0.282
	region (5)	-0.505	-0.910
	region (6)	-0.247	-0.663
downhill face	region (7)	-0.837	-0.830
	region (8)	-0.734	-0.758
	region (9)	-0.190	-0.232

Table 5 Normal stress

surface	region	model1	model2
		σ (Pa)	σ (Pa)
uphill face	region (1)	-0.030	0.041
	region (2)	-0.035	-0.094
	region (3)	-0.160	-0.223
top face	region (4)	0.071	0.389
	region (5)	0.018	0.054
	region (6)	0.007	0.038
downhill face	region (7)	-0.029	-0.005
	region (8)	-0.012	-0.004
	region (9)	-0.004	0.002

The friction drag was calculated by multiplying each wall shear stress by the area of each region and was converted into the value to the mainstream direction. The friction drag for the uphill face for model1 and model2 was 7.0×10^{-4}(N) and 6.3×10^{-4}(N). The friction drag for the top face was -8.2×10^{-4}(N) and -16.3×10^{-4}(N) for model1 and 2 respectively. The friction drag for the downhill face for both model1 and model2 was -4.5×10^{-4}(N). Therefore, there was a reduction in friction drag of 8.8×10^{-4}(N) for model2 when compared to model1. This result showed that there was a 1.8% reduction in friction drag when comparing the difference in the total drag between the flat surfaces and the wavy surfaces.

CONCLUSIONS

Measurements were conducted on the velocity field of turbulent boundary-layer flow over the truncated pyramids covered with flat surfaces and wavy surfaces and the total drag acting on these samples. The main conclusions obtained are as follows:

(1) The values of the total drag for the truncated pyramids covered with wavy surfaces were lower than those of the truncated pyramid covered with flat surfaces. The value of the total drag for the sample shaped with the values a=0.10mm, λ=2.86mm and a/λ=0.035 was 7.9% lower than that of the sample covered with flat surfaces.

(2) The value of the total drag was effectively reduced when the amplitude was a certain level and the value of the ratio of amplitude to wavelength for the wavy surfaces was a/λ=0.035.

(3) There was a 1.8% reduction in friction drag when comparing the difference in the total drag between the flat surfaces and the wavy surfaces.

REFERENCES

Etoh, T., Takehara, K. and Okamoto, K., 1999, "Performance evaluation of the PMC and the KC methods for particle extraction and tracking through their application to standard particle images" (in Japanese), *Transactions of Japan Society of Mechanical Engineers*, Vol. 65, Ser. B, 1688-1695.

Hjelmfelt Jr, A. T., Mockros, L. F., 1966, "Motion of discrete particles in a turbulent fluid", *Applied Scientific Research*, Vol. 16, 149-161.

Ishikawa, M. et al., 2000, "A novel algorithm for particle tracking velocimetry using the velocity gradient tensor", *Experiments in Fluids*, Vol. 29, 519-531.

Iwamoto, K., Suzuki, Y., Kasagi, N., 2002, "Reynolds number effect on wall turbulence: toward effective feedback control", *International Journal of Heat and Fluid Flow*, Vol. 23, 678-689.

Kitagawa, A., Hagiwara, Y., and Kouda, T., 2007, "PTV investigation of phase interaction in dispersed liquid-liquid two-phase turbulent swirling flow", *Experiments in Fluids*, Vol. 42, 871-880.

Kuroda, T., Yoshitake, N., Ozaki, Y., Hagiwara, Y., Kitagawa, A., 2009, “Turbulence and drag associated with water boundary-layer flow over wavy plates at a high Reynolds number “ *Proc. of 6th Symposium on Turbulent Heat and Mass Transfer*, 959-962.

Ozaki, Y., Yoshitake, N., Hagiwara, Y., 2009, “Drag acting on an angled-wavy plate by turbulent water flow at a high Reynolds number”, *Proc. of 6th Symposium on Turbulence and Shear Flow Phenomena*, 771-776.

Shintani, M., Yamasaki, R., Hagiwara, Y., 2012, “Swimming goggles development based on the measurement results of the total drag for turbulent water flow in an open channel” (in Japanese), *First Bio-inspired Manufacturing Symposium*, 1-4.

Yoshitake, N., Hagiwara, Y., Ozaki, Y., 2008, “Friction drag and pressure drag acting on an angled-wavy plate”, *Proc. of the 22nd Int. Congress of Theoretical and Applied Mechanics*, paper No.11760, 1-2.